Graphene Oxide—Polyelectrolyte Nanomembranes

Dhaval D. Kulkarni, Ikjun Choi, Srikanth S. Singamaneni, and Vladimir V. Tsukruk*

School of Material Science and Engineering, Georgia Institute of Technology, Atlanta, Georgia 30332-0245

ARTICLE

ABSTRACT Owing to its remarkable electrical, thermal, and mechanical properties, graphene, an atomic layer of carbon, is considered to be an excellent two-dimensional filler for polymer nanocomposites with outstanding mechanical strength along with the potential for excellent electrical and thermal properties. One of the critical limitations with conventional fillers is that the loading fraction required for achieving significant improvement in mechanical properties is relatively high, frequently reaching 50% for maximum strength. Here, we demonstrate that the mechanical properties of ultrathin laminated nanocomposites can be significantly enhanced by the incorporation of small amounts of a dense monolayer of planar graphene oxide (GO) flakes. Negatively charged functionalized graphene oxide layers were incorporated into polyelectrolyte multilayers (PEMs) fabricated in a layer-by-layer (LbL) assembly *via* Langmuir—Blodgett (LB) deposition. These LbL-LB graphene oxide nanocomposite films were released as robust freely standing membranes with large lateral dimensions (centimeters) and a thickness of around 50 nm. Micromechanical measurements showed enhancement of the elastic modulus by an order of magnitude, from 1.5 GPa for pure LbL membranes to about 20 GPa for only 8.0 vol % graphene oxide encapsulated LbL membranes. These tough nanocomposite PEMs can be freely suspended over large (few millimeters) apertures and sustain large mechanical deformations.

KEYWORDS: graphene · layer-by-layer assembly · free-standing · polymer nanocomposites · mechanical properties

Much of the initial excitement around graphene, a one-atom thick layer of sp^2-hybridized carbon atoms, is related to its unique electronic structure in which the electrons behave as Dirac fermions and ballistically conduct, thereby presenting an intriguing truly two-dimensional system.[1−4] With the introduction of robust chemical approaches (vapor[5,6] and solution[7−9]) for the large-scale synthesis of high-quality graphene, the real world application of this material excites the broader scientific community. For example, graphene has been suggested as an excellent candidate for nanoelectronic devices, solid-state gas sensors, ultrasensitive biodevices, and nanomechanical actuators, prominent among them being as a nanofiller in composite materials.[10−13] However, in order to use graphene as an efficient reinforcing component, it is paramount to incorporate nonaggregated and noncrumpled graphene sheets with maximum interfacial interactions for efficient load transfer within the polymer matrix.

Currently, multifunctional nanocomposites with improved mechanical performance are primarily fabricated by adding carbon nanotubes (CNTs),[14,15] inorganic nanoparticles,[16,17] and metal nanowires.[18−20] However, further development is hindered due to poor dispersion of these reinforcing nanostructures in the polymer matrix. Graphene on the other hand can be easily dissolved in a variety of solvents after its conversion to graphene oxide, which further helps in improving interfacial interactions with the polymer matrix.[13,21] Graphene oxide nanocomposites with thicknesses on the order of a few micrometers have been demonstrated to exhibit high mechanical strength combined with interesting physical properties, including good electrical and thermal conductivity and controlled electron transport.[22−26] Though these nanocomposites show a significant improvement in their mechanical properties, they still fall short of the expected theoretical numbers. Overcoming this critical limitation primarily relies on obtaining laminated and uncrumpled sheets of graphene finely dispersed into the polymer matrix. Even though graphene shows excellent intrinsic properties, the best among the known reinforcing agents, its full potential is yet to be witnessed.

Recently, highly ordered ultrathin membranes (50−100 nm) containing nanostructures showing high elasticity and robustness have been fabricated using layer-by-layer (LbL) assembly, cast at air−water interfaces, and spin-coated on a sacrificial layer. These membranes are known for

*Address correspondence to vladimir@mse.gatech.edu.

Received for review May 29, 2010 and accepted July 22, 2010.

Published online July 29, 2010. 10.1021/nn101204d

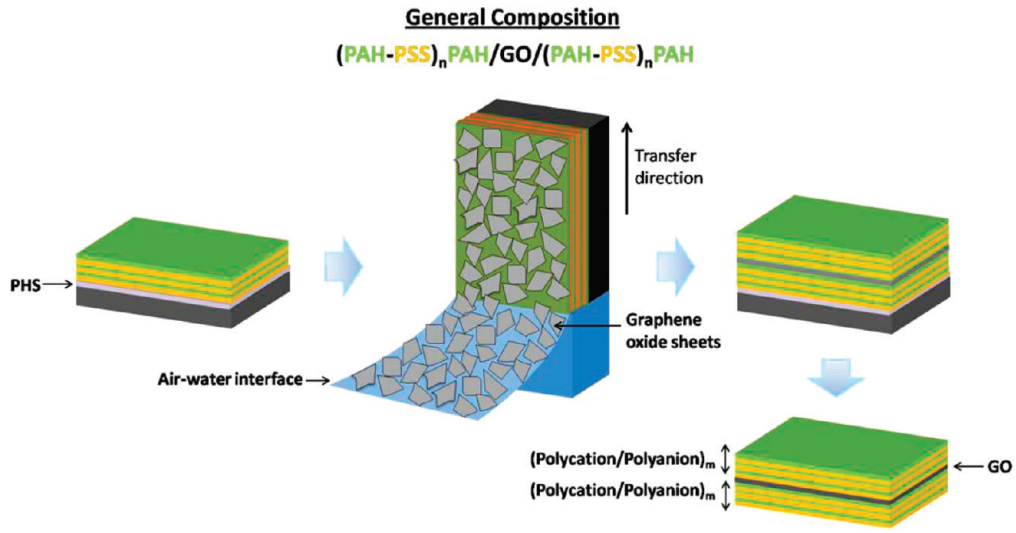

Figure 1. Schematic representation of fabrication and assembly of free-standing GO-LbL membrane.

controlled conformal orientation and stratification of the filler in the composite structure.[27−31] Excellent fracture toughness (~152 MJ/m^3) has been reported for CNT LbL nanocomposites.[32] A similar dramatic increase in the elastic modulus (~105 GPa) has been demonstrated for LbL nanocomposites with incorporated clay nanoplatelets with their content reaching 50 vol %.[33]

Here, we demonstrate the bottom-up fabrication of highly ordered, free-standing, layered nanocomposites with embedded graphene oxide sheets having excellent toughness and an improved elastic modulus, reaching 1.9 MJ/m^3 and 20 GPa, respectively, for a low content of graphene oxide (about 8%). Graphene oxide sheets were uniformly incorporated inside the LbL polyelectrolyte matrix, which provided a well-ordered stratification. In order to minimize the folding and wrinkling of the graphene oxide sheets, their deposition was performed using Langmuir−Blodgett (LB) technique instead of regular adsorption and spin-casting (Figure 1). Folding and wrinkling of graphene oxide sheets due to its flexible nature can be substantially minimized when deposited using LB technique.[34] These free-standing nanoscale (~50 nm thick) multilayered nanomembranes with a monolayer of planar graphene oxide flakes with large lateral dimensions (few centimeters across) possess outstanding mechanical robustness facilitating their easy handling and facile transfer to any appropriate substrate for further integration with microelectromechanical devices.

RESULTS AND DISCUSSION

Graphene oxide sheets prepared by the oxidative exfoliation of graphite flakes gave a homogeneous

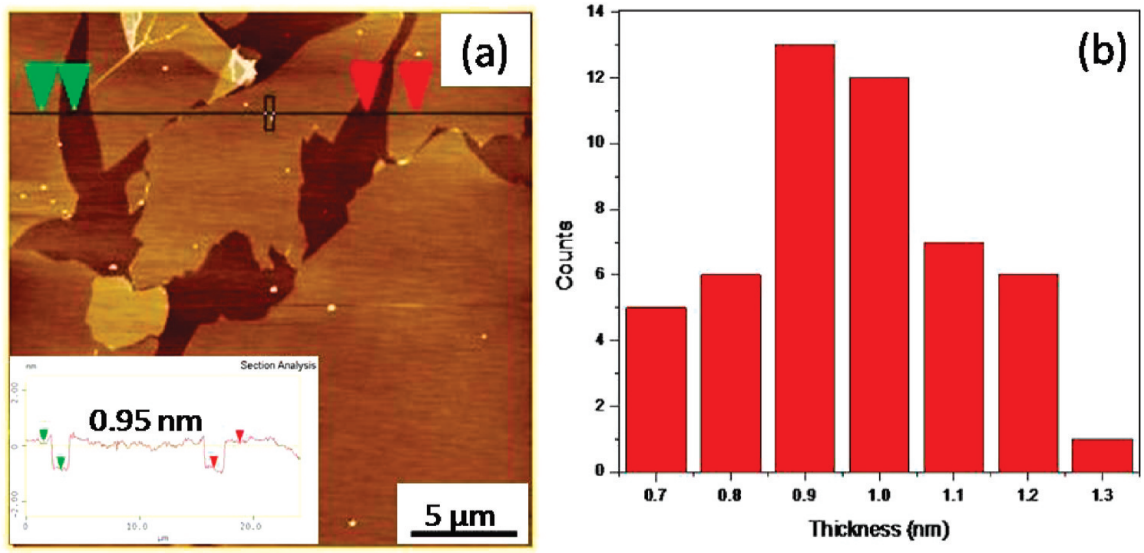

Figure 2. Characterization of graphene oxide sheets. (a) AFM image showing graphene oxide sheets deposited on silicon (inset showing the sectional image); *Z*-scale is 5 nm. (b) Histogram showing the variation of thickness for 50 different flakes with the average thickness of 0.96 ± 0.2 nm.

dispersion appropriate for single-layer deposition.[7] The concentration and size of the graphene oxide flakes were controlled by successive cycles of sonication followed by centrifugation. Sectional analysis of the AFM image revealed planar flakes up to a few tens of micrometers across having modest polydispersity in thickness, 0.96 ± 0.15 nm. Thus, most of the exfoliated flakes were single layers and bilayers[35−37] (Figure 2). In order to verify this, we built up a molecular model of graphene oxide sheets with surface functional groups by considering the ratio of C/O to be ~2.2 as reported by Hummers *et al.*[8] Simple calculations using van der Waals radii for epoxy and hydroxyl surface groups, bond lengths, and bond angles gave the effective thickness of a monolayer of graphene oxide to be 0.72 nm. Hydroxyl and epoxy groups in the basal plane primarily account for this increased thickness of GO compared to graphene (0.34 nm), whereas carboxyl groups known to be present at the edges contribute insignificantly. It is worth noting that reports on the thicknesses of graphene oxide sheets have suggested that the thicknesses of mono-, bi-, and trilayered graphene oxide sheets scale as 1:1.5:2.0, which is consistent with our estimations.[37]

Poly(allylamine hydrochloride) (PAH) and poly(sodium 4-styrene sulfonate) (PSS) PEMs fabricated here *via* spin-assisted LbL assembly showed uniform morphology with microroughness (within 1 × 1 μm^2) below 0.5 nm, common for LbL films.[38−40] The LB isotherm for graphene oxide solution showed a smooth rise in the surface pressure with a decrease in the surface area, suggesting an increase in the packing density of the graphene oxide (Figure 3). By controlling the surface pressure, surface coverage of the graphene oxide sheets was manipulated to give a uniform deposition with a high density reaching 90%, showing only occasional wrinkles and overlaps (Figure 3). High-resolution AFM imaging showed that the graphene oxide sheets followed the morphology of the polyelectrolyte layers (Figure 4a,b). The microroughness of graphene oxide sheets of 0.38 nm is indicative of atomic smoothness. High contrast in the phase image obtained at higher resolution showed large difference in surface properties of PEMs and graphene oxide sheets caused by their very different surface functionalities and stiffness (Figure 4c,d). These GO-LbL films with a total thickness within 50−70 nm depending upon composition and with 2 mm × 2 mm lateral dimensions were robust enough after being released to maintain their integrity during gentle handling, drying, and transfer onto different substrates. For instance, uniform deposition of GO-LbL membranes was obtained upon transfer onto a copper substrate with 150 μm aperture for further bulging mechanical tests and a PDMS compliant substrate for buckling mechanical tests (Figure 5).

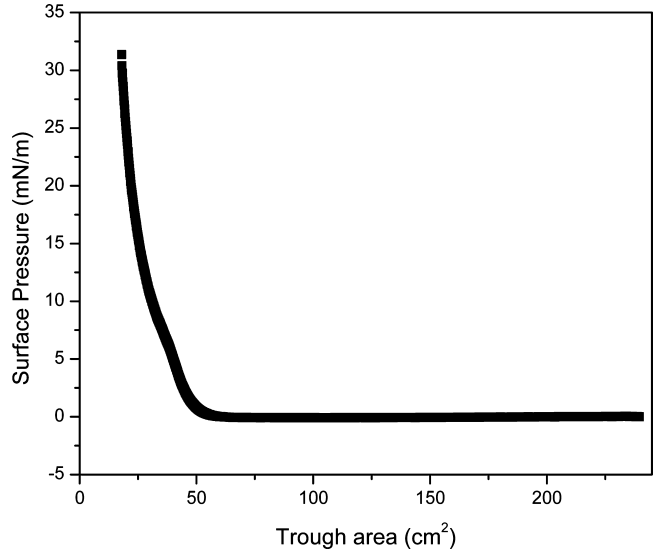

Figure 3. Langmuir isotherm for graphene oxide monolayer.

The elastic modulus of the membrane under compressive stresses was calculated using the equation given below.[14,18,41]

$$\lambda = 2\pi d\left(\frac{E_f(1-\nu_s^2)}{3E_s(1-\nu_f^2)}\right)^{1/3} \quad (1)$$

where λ is the periodicity of the buckles, ν_s,ν_f and E_s, E_f are Poisson's ratio and elastic modulus of the substrate (1.8 MPa) and film, respectively. The free-standing film transferred to elastomeric substrate showed a uniform buckling pattern with periodic wrinkles (λ) if the stress applied exceeded the threshold level (Figure 5a,b). The average value of λ determined from the 2D Fourier transform of optical images and AFM cross sections increased from 2.5 to 5.0 μm with increasing concentration of the graphene component and the corresponding Young's modulus increased from 1.5 to about 4.0 GPa (Table 1).

In the case of bulging measurements, a gradual increase in the applied pressure resulted in progressive membrane deflections as monitored with interference microscopy (Figure 5c,d). The bulging test measures the deflection d (μm) of a membrane subjected to a variable pressure P (Pa). The data obtained were analyzed using a theoretical model for a circular elastic plate clamped at stiff edges using equation given below:

$$P = P_0 + \left[C_0\frac{E}{1-\nu^2}\frac{h^4}{a^4} + C_1\frac{\sigma_0 h^2}{a^2}\right]\left(\frac{d}{h}\right) + C_2\frac{E}{1-\nu a^4}\frac{h^4}{a^4}\left(\frac{d}{h}\right)^3 \quad (2)$$

Here, P_0 is the initial pressure, E is the Young's modulus of the film, ν is its Poisson's ratio, h is the film thickness, a is the diameter of the membrane, d is the mem-

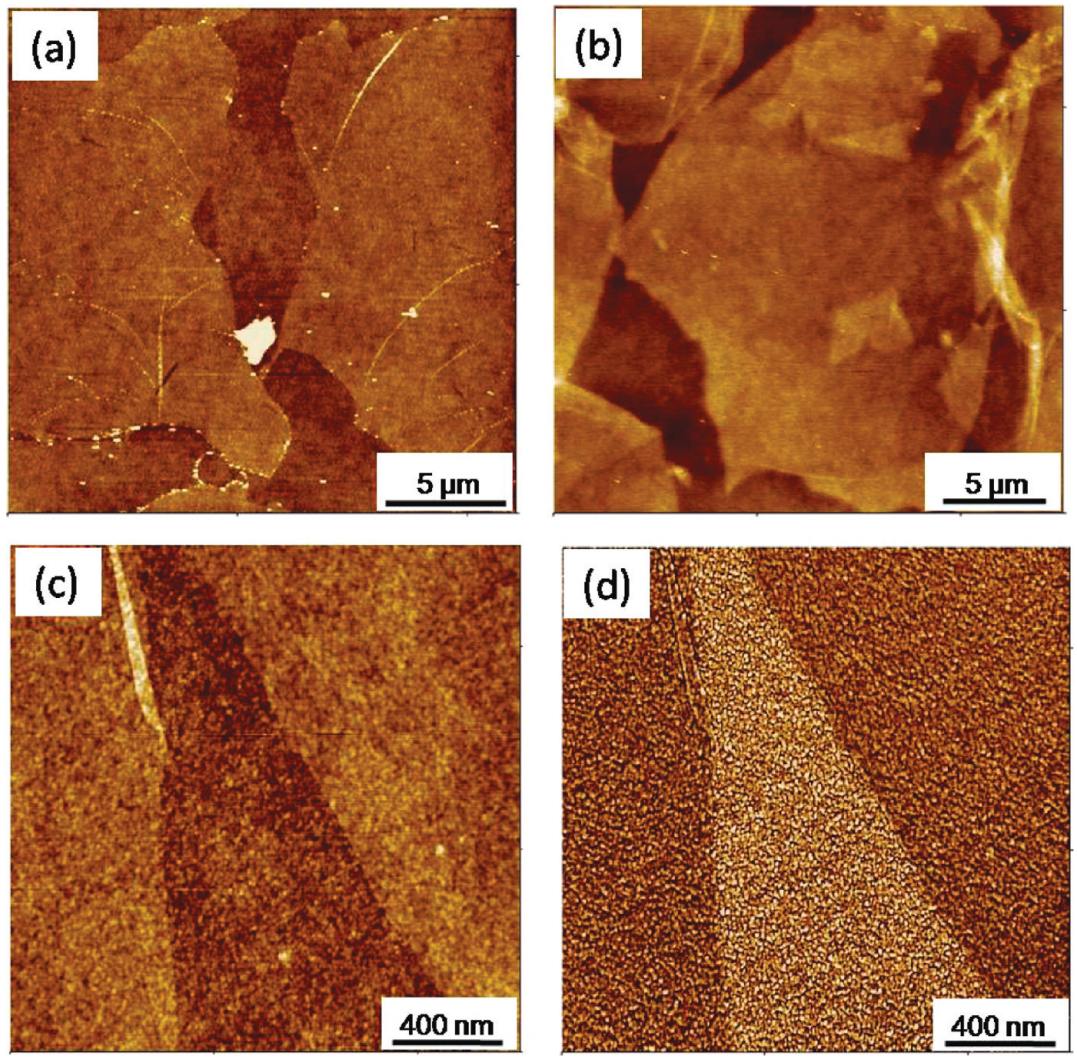

Figure 4. AFM images showing the morphology of GO-LbL membranes with (a) $(PAH/PSS)_9$ PAH−GO and (b) $(PAH/PSS)_9$ PAH−GO−PAH $(PSS/PAH)_9$ composition. High-resolution topography (c) and the corresponding phase image (d) of the membrane with $(PAH/PSS)_9$ PAH−GO composition; *Z*-scale for topographical images is 5 nm and for phase image is 5°.

brane deflection, and σ_0 is the residual stress. The tabulated coefficients C_0, C_1, and C_2 are found to be primarily dependent on the membrane geometry as discussed by Markutsya *et al.*[42] A full pressure *versus* deflection curve obtained from the bulging data was converted into a stress *versus* strain curve using the relationships $\sigma = Pr^2/4hd$ and $\varepsilon = 2d^2/3r^2$, where r is the radius of the opening (75 μm), d is the vertical deflection, and h is the film thickness.

The experimental data for the bulged membranes with different concentrations of graphene oxide component were fitted with the theoretical model for the determination of their Young's moduli in the elastic regime with other parameters (ultimate strength and toughness) calculated from stress−strain data derived from the bulging test (Figure 6).[42,43] For this analysis, the linear portion of the stress−strain curve, which reflects elastic deformation, can be fitted with the expression $\sigma = \sigma_0 + [E/(1 - \nu^2)]\varepsilon$ to calculate the elastic modulus. The Young's modulus increased from 1.5 GPa for original PEM to about 20 GPa with increasing graphene oxide loading from 1.7 to 8.0 vol % as will be discussed in detail below.

From the experimental data, it is worth noting a significant difference (about five times) in the elastic modulus obtained from buckling and bulging measurements, which is highly unusual for bulk composite materials (*e.g.*, 3.9 GPa *vs* 18.2 GPa for 8% GO content). Considering that our membranes were primarily incorporated with bilayer graphene oxide sheets, we suggest that the compressive stresses on the GO-LbL films initiate slippage and crumpling of the individual graphene oxide sheets at threshold compression. Indeed, the individual layers of the graphene oxide might slip past one another under shearing due to weaker van der Waals interactions of single layers within bilayers as compared to stronger interfacial interactions of graphene oxide sheets with PAH layers facilitated by polar interactions and hydrogen bonding be-

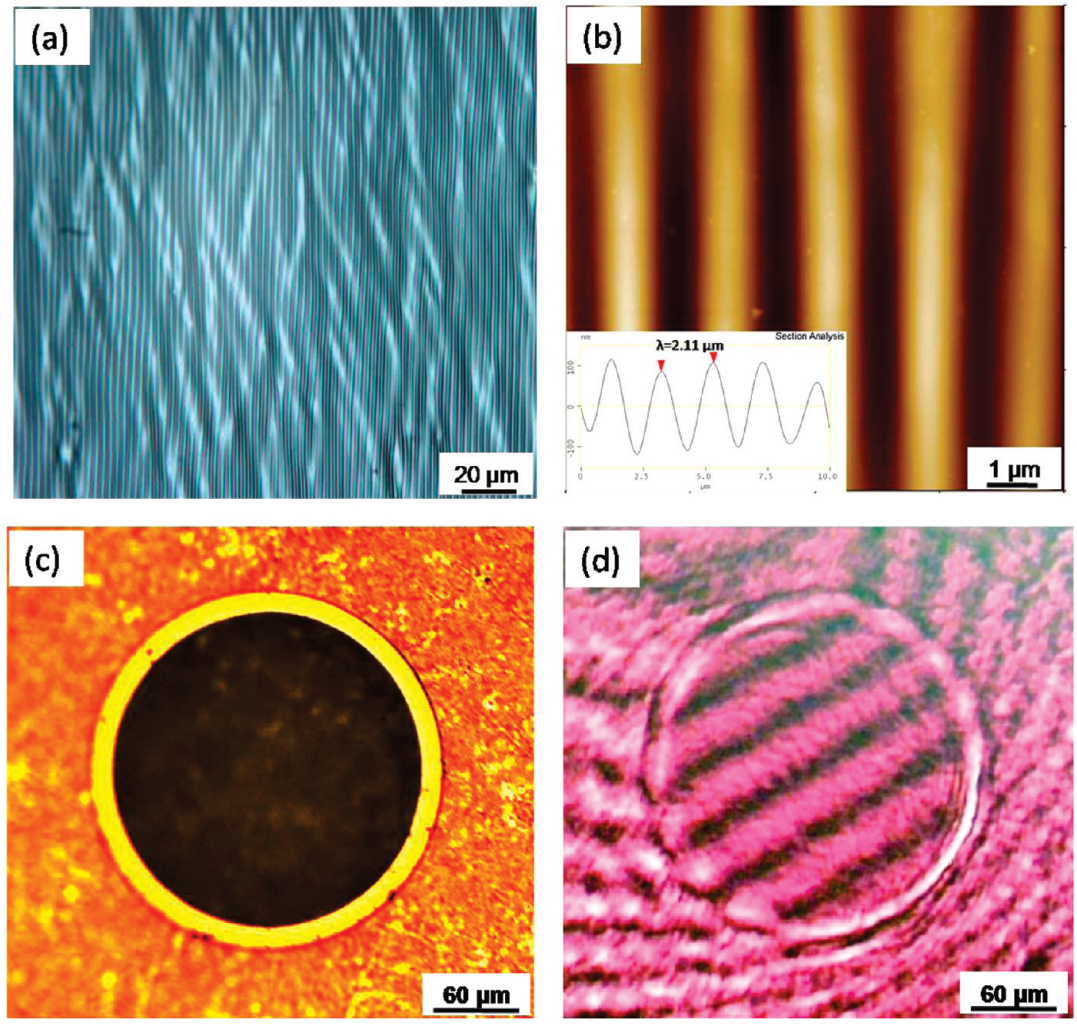

Figure 5. (a) Optical image of buckling pattern for LbL-LB film showing periodic wrinkles with spacing of 2.2 μm. (b) AFM image of the buckling pattern (inset showing the sectional image); *Z*-scale is 1 μm. (c) Optical image of the membrane suspended over a 150 μm copper aperture. (d) Interference pattern on the GO-LbL nanomembrane during bulging measurements.

tween epoxy/hydroxyl and amine groups. Due to the slippage and buckling, the stress applied is not completely transferred to the filler, and thus the reinforcing contribution of stiff but easily pliable graphene oxide sheets is significantly undermined, resulting in the compressive elastic modulus to be many-fold lower than the theoretical estimations (see below). On the contrary, in bulging measurements, the GO-LbL nanocomposites are subjected to tensile stress, which is evenly transferred across the thickness of the film. Thus, all of the graphene sheets contribute to the reinforcement fully with minimum slippage.

The stress−strain data derived from bulging measurements were used to estimate the ultimate strength, ultimate strain, and toughness in accor-

TABLE 1. Detailed Mechanical Properties of GO-Based Nanomembranes As Measured by Buckling and Bulging Techniques

				theoretical Young's modulus (GPa)	
volume fraction, φ (%)	effective membrane thickness (nm)	bulging Young's modulus (GPa)	buckling Young's modulus (GPa)	random orientation	parallel orientation
0	53 ± 2	1.9 ± 0.6	1.1 ± 0.5		
1.7	52 ± 2	4.5 ± 1.4	1.2 ± 0.5	3.1	5.6
3.3	48 ± 2	8.2 ± 0.7	2.2 ± 0.3	4.7	9.7
4.9	54 ± 2	10.4 ± 1.5	2.6 ± 0.4	6.2	13.6
6.4	62 ± 2	15.4 ± 1.5	2.8 ± 0.5	7.6	17.4
8.0	74 ± 2	18.2 ± 2.6	3.9 ± 0.5	9.0	21.0

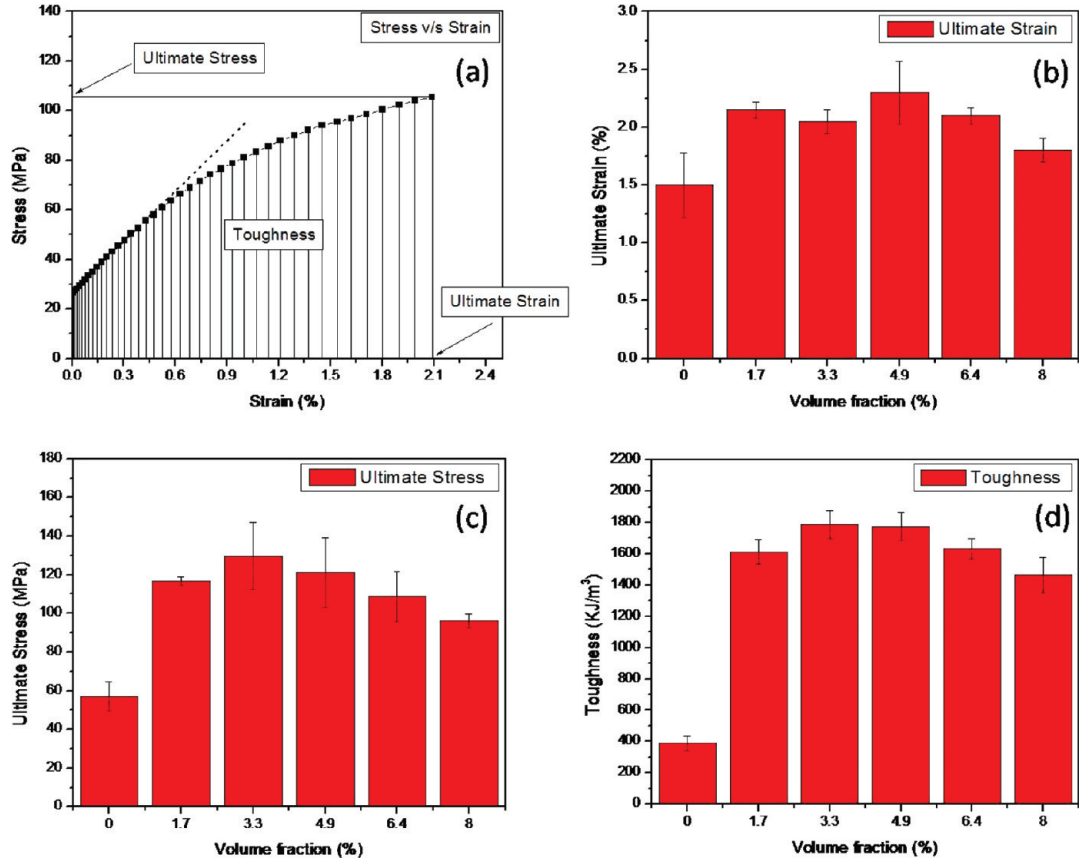

Figure 6. (a) Representative stress *vs* strain plot showing the ultimate strain, ultimate stress, and toughness values. Variation of (b) ultimate strain, (c) ultimate stress, and (d) toughness with the volume fraction of graphene oxide component.

dance with usual procedures.[29] This analysis showed that the ultimate strain increased significantly from 1.4% to 2.2% after incorporating graphene oxide sheets, indicating surprisingly higher flexibility of graphene oxide-containing nanocomposite membranes (Figure 6b). In contrast, polyelectrolyte membranes with 50 wt % CNTs have been shown to withstand an ultimate strain of 1%.[15] Moreover, PVA incorporated graphene oxide composites showed a 30% reduction in elasticity, whereas PVA/clay polyelectrolyte membrane showed an elasticity of 0.3%.[33,44] On the other hand, the ultimate mechanical strength of reinforced GO-LbL nanomembranes increased even more dramatically, by a factor 2.5, and reached 135 MPa (about 150 MPa for some specimens) for very low graphene oxide content (Figure 6c). Remarkably, the maximum mechanical strength value obtained at a minor loading of 3.3 vol % graphene oxide sheets is higher than that of "nacre" with extremely high content of inorganic laminates, one of the toughest known natural composites (~110 MPa).[28] Moreover, it is twice that of high-performance industrial plastics (20−70 MPa) and reaches 2/3 of that recorded for CNT-LbL membranes with 50 wt % loading of carbon nanotubes (220 MPa).[15]

An even more significant observation is that the toughness of the graphene oxide-containing nanomembranes (total energy required to fracture the specimen) increased dramatically, by almost 5-fold, up to about 1.9 MJ/m^3 (Figure 6d). The maximum toughness was again reached at very small 3.3 vol % content of the graphene oxide component due to the combination of higher mechanical strength and the ultimate strain. The outstanding value recorded here is about three times higher than those reported for other reinforced LbL films containing metal nanowires and nanoparticles[16,18] and for silk−clay LbL nanocomposites.[30]

To further verify the micromechanical parameters of the graphene oxide nanomembranes, theoretical predictions based upon the Halpin−Tsai model were directly compared with experimental data for nanocomposites with a variable content of graphene oxide sheets.[45] This model is widely applicable to a variety of reinforcement geometries specifically to individual platelets with random or parallel spatial arrangement of reinforcing nanostructures.

Theoretical values of Young's modulus under random and parallel orientation for different concentra-

tion of graphene oxide were calculated using Halpin−Tsai model with the following equations.[45]

$$E_{\text{random}} = \left[\frac{3}{8}\frac{1 + \left(\frac{2L_g}{T_g}\right)\eta_L V_g}{1 - \eta_L V_g} + \frac{5}{8}\frac{1 - 2\eta T V_g}{1 - \eta L V_g}\right]E_m \quad (3)$$

$$E_{\text{parallel}} = \left[\frac{1 + \left(\frac{2L_g}{T_g}\right)\eta_L V_g}{1 - \eta_L V_g}\right]E_m \quad (4)$$

$$\eta_L = \frac{\left(\frac{E_g}{E_m}\right) - 1}{\frac{E_g}{E_m} + 2L_g/T_g} \quad (5)$$

$$\eta_T = \frac{\left(\frac{E_g}{E_m}\right) - 1}{\frac{E_g}{E_m} + 2} \quad (6)$$

where, η_L and η_T are the Halpin−Tsai parameters reflecting the ratio of graphene oxide and matrix moduli in longitudinal and transversal directions, respectively. Young's modulus under random (E_{random}) and parallel (E_{parallel}) orientation was calculated by taking into account the graphene oxide aspect ratio (l/*d*), graphene oxide volume fraction (V_g), matrix modulus ($E_m = 1.5 \pm 0.5$ GPa for PAH/PSS film) and the modulus of graphene oxide ($E_g = 250$ GPa).[46]

The values thus obtained from the calculations for ideal parallel orientation of platelets and complete stress transfer scenario were remarkably close to those obtained experimentally from the bulging measurements (Figure 7). This correlation confirms that the design experimentally elaborated here reaches the theoretical limit of reinforcing effect with highly parallel graphene oxide sheets confined and uniformly distributed within a layered nanocomposite matrix.

It is worth noting that our attempts to assemble complete LbL nanocomposite films with graphene oxide flakes assembled as a step in LbL routine were not successful due to significant crumpling, folding, and aggregation of graphene flakes in an uncontrollable manner. The resulting fully LbL nanocomposites showed much less ordered and non-uniform morphology which compromised their ultimate properties with elastic modulus being only modestly (factor of 2−3) improved. On the other hand, multilayering of graphene oxide flakes by adding second, third, *etc.* LB layers and decreasing polyelectrolyte content did not show significant improvement, and overall mechanical properties were compromised by increasing brittleness.

Mechanical properties of reinforced nanocomposites with graphene oxide and graphite flakes incorporated in different polymer matrices have already been

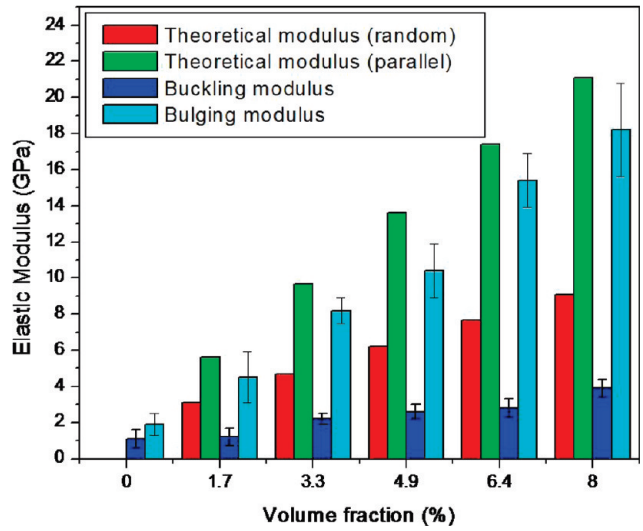

Figure 7. Plot showing the variation of elastic modulus calculated theoretically (under parallel and random orientation) and that calculated experimentally (using buckling and bulging measurements) with the volume fraction of graphene oxide.

reported in the literature. However, unlike this study, only modest to substantial reinforcing effect has been observed for highly heterogeneous morphologies.[47] For instance, Shi *et al.* demonstrated a 128% increase in the Young's modulus and 70% increase in the tensile strength of PVA−GO composites with 3 wt % graphene oxide.[44] Another study on PVA−GO composites reported a percolation threshold of 1.8 vol % for graphene oxide, beyond which the mechanical performance of the composite was reduced.[48] Graphene-containing films with a thickness between 5 and 10 μm showed an average modulus of 13 GPa with a tensile strength of 72 MPa.[49] Higher mechanical properties have usually been found for composites with extremely high content of graphene oxide sheets (*e.g.*, carbon paper) at the expense of the overall flexibility and uniformity.[24,26,50] Altogether, modest reinforcing effect is usually related to easy crumpling and wrinkling of this reinforcing component that compromises its reinforcing role.[51]

CONCLUSIONS

In conclusion, we demonstrated that functionalized graphene oxide layers incorporated into multilayered nanocomposites can be released as robust, freely standing membranes with large lateral dimensions (centimeters) and a thickness of around 50 nm. Micromechanical measurements showed dramatic enhancement of the elastic modulus to about 20 GPa for unusually low graphene oxide content. These tough nanocomposite PEMs can be freely suspended over large (few millimeters) apertures and sustain large mechanical deformations. It is worth noting that, although overall reinforcement effect and corresponding mechanical parameters achieved

here are much higher than those reported in the literature for composites with graphene oxides, they are still below record values for nanocomposites achieved with clay and carbon nanotubes.[15,32,33] However, contrary to these reinforcing nanostructures, which are difficult to disperse, graphene oxide can be dispersed in a wide range of solvents, which makes them compatible with a variety of materials. In addition, very high mechanical parameters can be achieved for very low loading rate (below 8%) in contrast to traditional bulk graphene-based composites with 50% and higher graphene content.

The most impressive aspect of free-standing graphene oxide reinforced nanomembranes reported here is their outstanding toughness. Considering that most applications demand better toughness along with a moderate increase in strength and elasticity, we suggest that these nanocomposite membranes would definitely serve this need. Electronic and thermal properties of graphene oxide sheets can be improved by chemical reduction or thermal annealing, but their subsequent compatibility with the polymer matrix is an issue yet to be addressed. Moreover, these nanocomposite membranes can find wider application due to their prospective electrical, thermal, and optical properties along with already outstanding mechanical properties unachievable in traditional clay-based nanocomposites. Electrically conductive, flexible, and robust membranes can provide an alternative to stiff silicon in capacitive pressure sensors used in MEMS devices. Also, these membranes can serve as a heat sink in electronic materials. We suggest that further studies on electrical and thermal conductivity, permeability, and utilization of other more compliant and high-performance matrices should be further performed to broaden the use of these promising nanomaterials.

EXPERIMENTAL SECTION

Chemicals and Materials: Graphene oxide was synthesized from natural graphite flakes (325 mesh, 99.8% metal basis) purchased from Alfa Aesar was perpared as per the Hummer's method. Stable dispersion of graphene oxide in a solution mixture of methanol/water (5:1) was subjected to ultrasonication for 15 min followed by centrifugation at 3000 rpm. The supernatant was decanted and used for LB experiments. Poly(4-vinylphenol) (PHS, M_w = 25 000), poly(allylamine hydrochloride) (PAH, M_w = 56 000), and poly(sodium 4-styrene sulfonate) (PSS, M_w = 70 000) were purchased from Aldrich and used as received. PAH was chosen due to the fact that the amine groups in the polymer will bind to the carboxyl and hydroxyl groups present in the graphene oxide. For LbL deposition, PAH (0.2 wt %) and PSS (0.2 wt %) solutions were prepared with Nanopure water (18 MΩU cm). The (100) silicon wafers of 10 × 20 mm were cleaned in piranha solution (3:1 mixture of H_2SO_4/H_2O_2) for 1 h and then rinsed thoroughly with Nanopure water.

Instrumentation: AFM images were collected using a Dimension-3000 instrument using silicon tips with tip radii between 15 and 20 nm and spring constant between 30 and 40 N/m.[52,53] The samples were scanned at 0.5−1.0 Hz for surface areas of 25 μm × 25 and 2.5 μm × 2.5 μm. The domain height and surface area coverage were determined from cross-sectional and bearing analysis, respectively. Langmuir isotherms at the air−water interface and LB deposition onto a silicon/LbL substrate were conducted at using a KSV 2000 LB minitrough according to the usual procedure.[54] Two milliliters of graphene oxide solution (0.1 g/L) in methanol/water mixture was uniformly distributed onto the water surface. The monolayer was deposited onto a clean silicon/LbL substrate at a surface pressure of 0.5 mN/m to obtain a uniform coverage.

Fabrication of LbL Films: The free-standing LbL membranes were prepared by a spin-assisted layer-by-layer (SA-LbL) assembly process, according to a procedure previously described in the literature.[14,18,42,55] Briefly, a 2.0 wt % solution of PHS in dioxane was spin-coated onto a clean silicon wafer. Alternating positive and negative PAH and PSS layers were spin-coated to form "*m*" bottom PAH/PSS bilayers terminated with PAH, followed by deposition of graphene oxide flakes using LB technique. Between casting steps, the coated surface was rinsed once again with Nanopure water. Another "*n*" PAH/PSS bilayers were assembled on the top. The concentration of the graphene oxide inside the polyelectrolyte matrix was manipulated by depositing graphene oxide sheets at regular intervals inside the matrix. Films with graphene oxide sandwiched between $(PAH/PSS)_m$PAH are designated as $(PAH/PSS)_m$PAH GO $(PAH/PSS)_n$ PAH (φ), where φ refers to the volume fraction of graphene oxide within the matrix. The volume fraction is calculated as the volume occupied by 2D graphene oxide sheets divided by the total volume of the membrane. The above procedure was performed in a class 100 clean air hood.

Finally, the LbL films were cut into approximately 2 mm × 2 mm squares using a stainless steel microneedle. They were then released by submersion in acetone, which preferentially dissolves the PHS layer. For easy deposition on a 3 mm diameter copper substrate with a 150 μm opening or a TEM grid, the floating membranes were transferred into another Petri dish containing Nanopure water. For thickness determination, some membranes were deposited on a silicon substrate and a micrometer wide scratch was made. The membrane thickness was measured by AFM cross-sectional analysis across the edge of the film or across the scratch mark.

Bulging Test: Bulging tests were performed according to procedures described in detail in the literature.[29,56] The bulging test data were analyzed using a model for the elastic deformation of circular membranes, according to the procedure described previously. The bulging tests were performed using a custom-made interferometer equipped with a charge-coupled device (CCD) camera (Logitech) and a He−Ne laser (λ = 632.8 nm). Pressures up to 6000 Pa were exerted using a 60 mL syringe regulated by an automatic pump (Kent Scientific Inc.) and monitored with an automatic pressure gauge, DPM 0.1 (SI Pressure Instruments).

The LbL membranes freely suspended over a copper substrate with a 150 μm aperture were first inspected under an optical microscope, and a minimal pressure was exerted to check for symmetrical Newton's ring patterns that indicate membrane homogeneity. While monitoring pressure, the slightly pressurized membrane was allowed to stand idle for a few minutes to ensure the absence of any leaks. The mounted membrane was then tilted at a minimum angle, θ, to form a vertical interference pattern. For bulging measurements conducted between 0 and 6000 Pa, the maximum membrane deflection did not exceed 8 μm. Under these conditions, the maximum error due to tilting was about 6 nm, which is within the resolution of the interference pattern (1/4λ or 160 nm). During measurements, a transparent crosshair window was laid over the digital image of the membrane such that the central vertical interference pattern coincided with the vertical line of the crosshair. As the pressure increased, the interference pattern moved laterally across the crosshair. Concomitantly, the deflection of the copper substrate was also monitored using a mouse cursor as the target marker. A minimum of three randomly selected specimens were measured for each membrane with different densities of graphene oxide.

Buckling Test: Buckling tests were conducted to independently evaluate the elastic modulus of LbL membranes.[41,57] For an isotropic thin membrane, a uniform buckling pattern with a characteristic wavelength, λ, was observed when subjected to a critical compressive stress.[58] The spacing of this pattern, which is directly related to the elastic modulus, was calculated using AFM and verified from optical images (Figure 5). To initiate the buckling pattern, a 2 mm × 2 mm membrane piece was placed over a 0.6 cm × 0.6 cm × 0.4 cm PDMS substrate, which was slowly compressed with micrometer-sized increments. The total compressive distance was generally less than 15 μm. The compression was monitored in differential interference contrast (DIC) mode adjusted for maximum contrast. Optical images were captured with a Leica MZ16 microscope.

Acknowledgment. This work is supported by the Semiconductor Research Corporation and Air Force Office for Scientific Research.

REFERENCES AND NOTES

1. Giem, A. K.; Novoselov, K. S. The Rise of Graphene. *Nat. Mater.* **2007**, *6*, 183–191.
2. Rao, C. N. R.; Sood, A. K.; Subramanyam, K. S.; Govindraj, A. Graphene: The New Two-Dimensional Nanomaterial. *Angew. Chem., Int. Ed.* **2009**, *28*, 7752–7777.
3. Novoselov, K. S.; Jiang, D.; Schedin, F.; Booth, T. J.; Khotkevich, V. V.; Morozov, S. V.; Giem, A. K. Two-Dimensional Atomic Crystals. *Proc. Natl. Acad. Sci. U.S.A.* **2005**, *102*, 10451–10453.
4. Novoselov, K. S.; Giem, A. K.; Morozov, S. V.; Jiang, D.; Katsnelson, M. I.; Grigorieva, I. V.; Dubonos, S. V.; Firsov, A. A. Two-Dimensional Gas of Massless Dirac Fermions in Graphene. *Nature* **2005**, *438*, 197–200.
5. Reina, A.; Thiele, S.; Jia, X.; Ho, J.; Nezich, D.; Son, H.; Bulovic, V.; Dresselhaus, M. S.; Kong, J. Large Area, Few Layer Graphene Films on Arbitrary Substrates by Chemical Vapor Deposition. *Nano Lett.* **2009**, *9*, 30–35.
6. Wei, D.; Liu, Y.; Wang, Y.; Zhang, H.; Huang, L.; Yu, G. Synthesis of N-Doped Graphene by Chemical Vapor Deposition and Its Electrical Properties. *Nano Lett.* **2009**, *9*, 1752–1758.
7. Park, S.; Ruoff, R. S. Chemical Methods for the Production of Graphenes. *Nat. Nanotechnol.* **2009**, *4*, 217–224.
8. Hummers, W. S.; Offeman, R. E. Preparation of Graphitic Oxide. *J. Am. Chem. Soc.* **1958**, *80*, 1339.
9. Tung, V. C.; Allen, M. J.; Yang, Y.; Kaner, R. B. High-Throughput Solution Processing of Large-Scale Graphene. *Nat. Nanotechnol.* **2009**, *4*, 25–29.
10. Bunch, J. S.; Zande, V.; Verbridge, S. S.; Frank, I. W.; Tanebaum, D. M.; Parpia, J. M.; Craighead, H. G.; McEuen, P. L. Electromechanical Resonators from Graphene Sheets. *Science* **2007**, *315*, 490–493.
11. Park, S.; An, J.; Suk, J. W.; Ruoff, R. S. Graphene Based Actuators. *Small* **2009**, *6*, 210–222.
12. Schedin, F.; Giem, A. K.; Morozov, S. V.; Hill, E. W.; Blake, P.; Katsnelson, M. I.; Novoselov, K. S. Detection of Individual Gas Molecules Adsorbed on Graphene. *Nat. Mater.* **2007**, *6*, 652–655.
13. Stankovich, S.; Dikin, D. A.; Dommett, G. H. B.; Kohlhass, K. M.; Zimney, E. J.; Stach, E. A.; Piner, R. D.; Nguyen, S. T.; Ruoff, R. S. Graphene Based Composite Materials. *Nat. Nanotechnol.* **2009**, *4*, 217–224.
14. Ko, H.; Jiang, C.; Shulha, H.; Tsukruk, V. V. Carbon Nanotubes Encapsulated into Freely Suspended Flexible Films. *Chem. Mater.* **2005**, *17*, 2490–2493.
15. Mamedov, A. A.; Kotov, N. A.; Prato, M.; Guldi, D. M.; Wickstead, J. P.; Hirsh, A. Molecular Design of Strong SWNT/Polyelectrolyte Multilayer Composites. *Nat. Mater.* **2004**, *3*, 721–728.
16. Ko, H.; Jiang, C.; Tsukruk, V. V. Encapsulating Nanoparticle Arrays into Layer-by-Layer Multilayers by Capillary Transfer Lithography. *Chem. Mater.* **2005**, *17*, 5489–5497.
17. Mamedov, A. A.; Kotov, N. A. Free-Standing Layer-by-Layer Assembled Films of Magnetite Nanoparticles. *Langmuir* **2000**, *16*, 5530–5533.
18. Gunawidjaja, R.; Jiang, C.; Pelshanko, S.; Ornatska, M.; Singamaneni, S.; Tsukruk, V. V. Flexible and Robust 2D Arrays of Silver Nanowires Encapsulated within Freestanding Layer-by-Layer Films. *Adv. Funct. Mater.* **2006**, *16*, 2024–2034.
19. Aroca, R. F.; Goulet, P. J. G.; dos Santos, D. S.; Alvarez-Puebla, R. A.; Oliveira, O. N. Silver Nanowire Layer-by-Layer Films as Substrates for Surface-Enchanced Raman Scattering. *Anal. Chem.* **2005**, *77*, 378–382.
20. Kovtyukhova, N. I.; Marin, B. R.; Mbindyo, J. K. N.; Smith, P. A.; Razavi, B.; Mayer, T. S.; Mallouk, T. E. Layer-by-Layer Assembly of Rectifying Junctions in and on Metal Nanowires. *J. Phys. Chem. B* **2001**, *105*, 8762–8769.
21. Fang, M.; Wang, K.; Lu, H.; Yang, Y.; Nutt, S. Covalent Polymer Functionalization of Graphene Nanosheets and Mechanical Properties of Composites. *J. Mater. Chem.* **2009**, *19*, 7098–7105.
22. Chen, H.; Muller, M. B.; Gilmore, K. J.; Wallace, G. G.; Li, D. Mechanically Strong, Electrically Conductive and Biocompatible Graphene Paper. *Adv. Mater.* **2008**, *20*, 3557–3661.
23. Chen, C.; Yang, Q.; Yang, Y.; Lv, W.; Wen, Y.; Hou, P.; Wang, M.; Cheng, H. Self-Assembled Free-Standing Graphite Oxide Membrane. *Adv. Mater.* **2009**, *21*, 3007–3011.
24. Park, S.; Dikin, D. A.; Nguyen, S. T.; Ruoff, R. S. Graphene Oxide Sheets Chemically Cross-Linked by Polyallylamine. *J. Phys. Chem. C* **2009**, *113*, 15801–15804.
25. Rafiee, M. A.; Rafiee, J.; Wang, Z.; Song, H.; Yu, Z.; Koratkar, N. Enhanced Mechanical Properties of Nanocomposites at Low Graphene Content. *ACS Nano* **2009**, *3*, 3884–3890.
26. Dikin, D. A.; Stankovich, S.; Zimney, E. J.; Piner, R. D.; Dommett, G. H. B.; Evmenenko, G.; Nguyen, S. T.; Ruoff, R. S. Preparation and Characterization of Graphene Oxide Paper. *Nature* **2007**, *448*, 457–460.
27. Lutkenhaus, J. L.; Hrabak, K. D.; McEnnis, K.; Hammond, P. T. Elastomeric Flexible Free-Standing Hydrogen-Bonded Nanoscale Assemblies. *J. Am. Chem. Soc.* **2005**, *127*, 17228–17234.
28. Tang, Z.; Kotov, N. A.; Magonov, S.; Ozturk, B. Nanostructured Artificial Nacre. *Nat. Mater.* **2003**, *2*, 413–148.
29. Jiang, C.; Markutsya, S.; Pikus, Y.; Tsukruk, V. V. Freely Suspended Nanocomposite Membranes as Highly Sensitive Sensors. *Nat. Mater.* **2004**, *3*, 721–728.
30. Kharlampieva, E.; Kozlovskaya, V.; Gunawidjaja, R.; Shevchenko, V.; Vaia, R.; Naik, R.; Kaplan, D.; Tsukruk, V. V. Flexible Silk-Inorganic Nanocomposites: From Transparent to Highly Reflective. *Adv. Funct. Mater.* **2010**, *20*, 840–846.
31. Gunawidjaja, R.; Jiang, C.; Peleshanko, S.; Ornatska, M.; Singamaneni, S.; Tsukruk, V. V. Flexible and Robust 2D Arrays of Silver Nanowires Encapsulated within Freestanding Layer-by-Layer Films. *Adv. Funct. Mater.* **2006**, *16*, 2024–2034.
32. Shim, B. S.; Zhu, J.; Jan, E.; Critchley, K.; Ho, S.; Podsiadlo, P.; Sun, K.; Kotov, N. A. Multiparameter Structural Optimization of Single-Walled Carbon Nanotube Composites: Towards Record Strength, Stiffness, and Toughness. *ACS Nano* **2009**, *3*, 1711–1722.
33. Podsiadlo, P.; Kaushik, A. K.; Arruda, E. M.; Waas, A. M.; Shim, B. S.; Xu, J.; Nandivada, H.; Pumplin, B. G.; Lahann, J.; Ramamoorthy, A.; Kotov, N. A. Ultrastrong and Stiff Layered Polymer Nanocomposites. *Science* **2007**, *318*, 80–83.
34. Cote, L. J.; Kim, F.; Huang, J. Langmuir−Blodgett Assembly of Graphite Oxide Single Layers. *J. Am. Chem. Soc.* **2009**, *131*, 1043–1049.
35. Medhekar, N. V.; Ramasubramaniam, A.; Ruoff, R. S.; Shenoy, V. B. Hydrogen Bond Networks in Graphene Oxide Composite Paper: Structure and Mechanical Properties. *ACS Nano* **2010**, *4*, 2300–2306.
36. Nakajima, T.; Mabuchi, A.; Hagiwara, R. A New Structural Model of Graphite Oxide. *Carbon* **1988**, *26*, 357–361.
37. Mkhoyan, A. K.; Contryman, A. W.; Silcox, J.; Stewart, D. A.;

Eda, G.; Mattevi, C.; Miller, S.; Chhowala, M. Atomic and Electronic Structure of Graphene-Oxide. *Nano Lett.* **2009**, *9*, 1058–1063.
38. Jiang, C. Y.; Tsukruk, V. V. Free Standing Nanostructures *via* Layer-by-Layer Assembly. *Adv. Mater.* **2006**, *18*, 829–840.
39. Jiang, C. Y.; Tsukruk, V. V. Organized Arrays of Nanostructures in Freely Suspended Nanomembranes. *Soft Matter* **2005**, *1*, 334–337.
40. Jiang, C. Y.; Markutsya, S.; Tsukruk, V. V. Compliant, Robust, and Truly Nanoscale Free-Standing Multilayer Films Fabricated Using Spin-Assisted Layer-by-Layer Assembly. *Adv. Mater.* **2004**, *16*, 157–161.
41. Volynskii, A. L.; Bazhenov, S.; Lebedeva, O. V.; Bakeev, N. F. Mechanical Buckling Instability of Thin Coatings Deposited on Soft Polymer Surfaces. *J. Mater. Sci.* **2000**, *35*, 547–554.
42. Markutsya, S.; Jiang, C.; Pikus, Y.; Tsukruk, V. V. Free-Standing Multilayered Nanocomposites Films as Highly Sensitive Nanomembranes. *Adv. Funct. Mater.* **2005**, *15*, 771–780.
43. Jiang, C.; Markutsya, S.; Shulha, H.; Tsukruk, V. V. Freely Suspended Gold Nanoparticles Arrays. *Adv. Mater.* **2005**, *17*, 1669–1673.
44. Xu, Y.; Hong, W.; Bai, H.; Li, C.; Shi, G. Strong and Ductile Poly(vinyl alcohol)/Graphene Oxide Composite Films with a Layered Structure. *Carbon* **2009**, *47*, 3538–3543.
45. Agarwal, D. D.; Broutman, L. J. *Analysis and Performance of Fiber Composites*, 2nd ed.; Wiley: New York, 1990.
46. Gomez-Navarro, C.; Burghard, M.; Kern, K. Elastic Properties of Chemically Derived Single Graphene Sheets. *Nano Lett.* **2008**, *8*, 2045–2049.
47. Kovtyukhova, N. I.; Ollivier, P. J.; Martin, B. R.; Mallouk, T. E.; Chizhik, S. A.; Buzaneva, E. V.; Gorchinskiy, A. D. Layer-by-Layer Assembly of Ultrathin Composite Films from Micron-Sized Graphite Oxide Sheets and Polycations. *Chem. Mater.* **1999**, *11*, 771–778.
48. Zhao, X.; Zhang, Q.; Chen, D. Enhanced Mechanical Properties of Graphene-Based Poly(vinyl alcohol) Composites. *Macromolecules* **2010**, *43*, 2357–2363.
49. Chen, C.; Yang, Q.; Yang, Y.; Lv, W.; Wen, Y.; Hou, P.; Wang, M.; Cheng, H. Self-Assembled Free-Standing Graphite Oxide Membrane. *Adv. Mater.* **2009**, *21*, 3007–3011.
50. Shen, J.; Hu, Y.; Li, C.; Qin, C.; Shi, M.; Ye, M. Layer-by-Layer Self-Assembly of Graphene Nanoplatelets. *Langmuir* **2009**, *25*, 6122–6128.
51. Kim, H.; Macosko, C. W. Morphology and Properties of Polyester/Exfoliated Graphite Nanocomposites. *Macromolecules* **2008**, *41*, 3317–3327.
52. Tsukruk, V. V. Scanning Probe Microscopy of Polymer Surfaces. *Rubber Chem. Technol.* **1997**, *70*, 430–467.
53. Tsukruk, V. V.; Reneker, D. H. Scanning Probe Microscopy of Organic and Polymeric Films: From Self-Assembled Monolayers to Composite Materials. *Polymer* **1995**, *36*, 1791–1808.
54. Peleshanko, S.; Jeong, J.; Gunawidjaja, R.; Tsukruk, V. V. Amphiphilic Heteroarm PEO-*b*-PS_m Star Polymers at the Air−Water Interface: Aggregation and Surface Morphology. *Macromolecules* **2004**, *37*, 6511–6522.
55. Cho, J.; Char, K.; Hong, J.; Lee, K. Fabrication of Multilayer Films Using Spinning Process. *Adv. Mater.* **2001**, *13*, 1076–1078.
56. Mallwitz, F.; Goedel, W. A. Physically Cross-Linked Ultrathin Elastomeric Membranes. *Angew. Chem., Int. Ed.* **2001**, *40*, 2645–2647.
57. Stafford, C. M.; Harrison, C.; Beers, K. L.; Karim, A.; Amis, E. J.; Vanlandingham, M. R.; Kim, H. C.; Volksen, W.; Miller, R. D.; Simonyi, E. E. A Buckling-Based Metrology for Measuring the Elastic Moduli of Polymeric Thin Films. *Nat. Mater.* **2004**, *3*, 545–550.
58. Jiang, C.; Singamaneni, S.; Merrick, E.; Tsukruk, V. V. Complex Buckling Instability Patterns of Nanomembranes with Encapsulated Gold Nanoparticle Arrays. *Nano Lett.* **2006**, *6*, 2254–2259.